

## MIT Open Access Articles

*An Asymmetric Iron#Based Redox#Active System for Electrochemical Separation of Ions in Aqueous Media*

The MIT Faculty has made this article openly available. **Please share** how this access benefits you. Your story matters.

**Citation:** Tan, Kai#Jher, Su, Xiao and Hatton, T. Alan. 2020. "An Asymmetric Iron#Based Redox#Active System for Electrochemical Separation of Ions in Aqueous Media." *Advanced Functional Materials*, 30 (15).

**As Published:** <http://dx.doi.org/10.1002/adfm.201910363>

**Publisher:** Wiley

**Persistent URL:** <https://hdl.handle.net/1721.1/140934>

**Version:** Author's final manuscript: final author's manuscript post peer review, without publisher's formatting or copy editing

**Terms of use:** Creative Commons Attribution-Noncommercial-Share Alike



# An asymmetric iron-based redox-active system for electrochemical separation of ions in aqueous media

*Kai-Jher Tan, Xiao Su, and T. Alan Hatton\**

K.-J. Tan, Dr. X. Su<sup>[+]</sup>, Prof. T. A. Hatton

Department of Chemical Engineering

Massachusetts Institute of Technology

77 Massachusetts Avenue, Cambridge, MA, 02139, USA

E-mail: [tahatton@mit.edu](mailto:tahatton@mit.edu)

<sup>[+]</sup>Present Address: Department of Chemical and Biomolecular Engineering

University of Illinois at Urbana-Champaign

600 South Mathews Avenue, Urbana, IL, 61801, USA

Keywords: electrochemical separations, asymmetric electrodes, ferrocene, hexacyanoferrate, heavy metal oxyanions

This is the author manuscript accepted for publication and has undergone full peer review but has not been through the copyediting, typesetting, pagination and proofreading process, which may lead to differences between this version and the [Version of Record](#). Please cite this article as [doi: 10.1002/adfm.201910363](https://doi.org/10.1002/adfm.201910363).

This article is protected by copyright. All rights reserved.

Electrochemically-mediated redox-active processes are gaining momentum as a promising liquid-phase separation technology. Compared to conventional systems, they offer potential benefits such as smaller energy footprints, non-destructive operation, reversibility, and tunability for specific analyte removal, with clear applications to societal and industrial challenges like water treatment and chemical synthesis. In this study, an asymmetric Faradaic cell heterogeneously functionalized with a metallopolymer at the anode and a hexacyanoferrate material at the cathode is presented for the first time. The redox-active species' iron centers enhance the electrosorption of heavy metal oxyanions (HMOA) with up to 98% removal in the ppb range, and offer tunable operating windows as low as ca. 0.1 V at 1 A/m<sup>2</sup>. By avoiding water splitting, the hexacyanoferrate cathode imparts additional advantages, namely, a four-fold reduction in adsorption energy requirements, full suppression of solution pH increase, and the ability to capture redox-active catalytic anions such as polyoxometalates (POM) without altering their bulk oxidation state. This hybrid framework of a polymeric ferrocene anode and crystalline hexacyanoferrate cathode allows for simultaneous and synergistic uptake of anions and cations, respectively, creating a new asymmetric scheme for water-based separations, with foreseeable future extension to fields such as ion-sensing, energy storage, and electrocatalysis.

## 1. Introduction

Chemical separations are of crucial importance to, and are used ubiquitously in, the production of commodity chemicals and valuable species. However, as the purification steps in industrial manufacturing are often highly material and energy-intensive, there is a clear urgency for pursuing green engineering to develop and implement clean energy-efficient separation processes to reduce the economic and environmental impacts of high global energy consumption.<sup>[1]</sup> Separations are also critically relevant in aqueous media, particularly in the areas of environmental remediation and drinking water. Freshwater scarcity systemically affects four billion people,<sup>[2]</sup> with water pollution rendering more than 1 billion people without access to clean water. With global water demand expected to increase with population growth, the availability of low cost and low energy water purification methods is imperative.<sup>[3]</sup>

Electrochemical processes are emerging as an attractive platform for water remediation, as they do not require the chemical solvent regenerants or direct heat and pressure inputs often found in conventional techniques such as ion exchange, distillation, or membrane filtration methods. The modularity of the electrical stimulus allows the technology to be automated remotely and compactly designed, with adjustability to variable contaminant concentrations.<sup>[4]</sup> Electrochemistry has been used in the electro-coagulation/flotation/deposition of heavy metal ions,<sup>[5]</sup> electro-Fenton processes for aromatic degradation<sup>[6]</sup> and electroreduction of nitrosamines,<sup>[7]</sup> as well as in separation techniques such as electrochemical ion exchange (EIX), where solution pH changes from water splitting activate and deactivate the ion-exchange materials,<sup>[8]</sup> and capacitive deionization (CDI), where salt ions are adsorbed within the electrical double layers established at the electrode surfaces.<sup>[9]</sup>

The electrochemical reactions occurring at the electrodes can be further enhanced by leveraging the pseudocapacitance of redox-active materials, which provides variable Faradaic charges based on electrochemical potential to enhance adsorption capacity.<sup>[10]</sup> To this end, electroactive polymers and inorganic materials have been used for energy storage applications in supercapacitors and batteries,<sup>[11]</sup> as well as electrochemically-mediated aqueous separations.<sup>[12]</sup> Electrochemically-mediated separation processes are especially attractive since electrochemical degradation techniques can often be energetically expensive, and can create unwanted by-products.<sup>[6]</sup> Of particular note is that electrochemical separation processes can be designed for molecular targeting in selectively removing certain species where methods such as distillation and chromatography may be inefficient,<sup>[4]</sup> a concept that has previously been used in the development of ion-selective electrochemical sensors.<sup>[13]</sup>

The quintessential redox-active species is ferrocene, a stable, 18-electron organometallic molecule first discovered in 1951, and the prototypical example of the metallocene class of sandwich compounds.<sup>[14]</sup> The synthesis of the ferrocene homopolymer, poly(vinylferrocene) (PVFc), was reported shortly afterwards in 1955.<sup>[15]</sup> The redox-active properties as well as the accompanying structural changes of PVFc have been studied in different solvent and electrolyte environments.<sup>[16]</sup> Of particular interest is the interaction affinity of the oxidized cationic form of PVFc, poly(vinylferrocenium) (PVFc<sup>+</sup>), with anions other than those of the supporting electrolyte. The PVFc metallopolymer has recently been observed to exhibit redox-mediated hydrogen bonding that imparts it with the ability to electrochemically separate organic carboxylate anions in both aqueous and organic solution with high separation factors of ca. 100 in over 100-fold excess competing electrolyte,<sup>[17]</sup> inorganic oxyanions from wastewater<sup>[18]</sup> and nuclear waste,<sup>[19]</sup> and even proteins.<sup>[20]</sup> As the activation of the redox-species is mediated by an electrochemical stimulus, the process is reversible and desorption of adsorbed compounds can be accomplished via moderate electrochemical potential swings. This framework for targeted and electrochemically-reversible separation has been applied to both organic micropollutants such as pharmaceuticals and personal care products (PPCPs) and endocrine disruptors,<sup>[21]</sup> which are usually present in the ppt to ppb concentration ranges and inefficiently removed to varying degrees in wastewater plants,<sup>[22]</sup> as well as inorganic heavy metal contaminants, which are well-known for their toxicity and carcinogenicity.<sup>[23]</sup>

During electrochemical anion adsorption in aqueous media, the oxidation of PVFc can be balanced by water reduction at the counter electrode with an inert cathode material like carbon or platinum. However, this process not only increases energy requirements due to the reduction

potential of water (thermodynamic potential of -0.41 V vs SHE at pH 7) and subsequent current leakage,<sup>[24]</sup> but also changes the solution chemistry through basification, which can severely impact separation performance due to the fouling of PVFc<sup>+</sup> active sites by nucleophilic hydroxide anions<sup>[21, 25]</sup> or even chemical degradation of the ferrocene moieties.<sup>[26]</sup> Carbonaceous electrodes are widely employed in CDI processes for salt electrosorption, where typical operating potential windows can reach as high as 1 to 1.4 V, but significant improvements in salt adsorption capacity have been observed when Faradaic species are used over purely capacitive materials.<sup>[9b, 24, 27]</sup> To maintain the modularity of the electrochemical cell, the cathode can be functionalized with a Faradaic species to act as an electron sink, yielding an asymmetric electrochemical system. Furthermore, the cathodic species becomes a source of electrons for the reduction of the ferrocenium moieties during the desorption step, enabling efficient electron utilization in a complete electroswing cycle. Dual configurations involving PVFc and different cobalt-containing metallopolymer have been previously used to effectively suppress pH increases in the solution, as well as facilitate in-tandem separation of both anionic and cationic species.<sup>[21]</sup> However, the complexity of these cathodic metallopolymer can pose difficulties in effective process scale-up.

As such, the motivation of this work is to investigate the use of alternative reducing compounds which are less expensive and can be more easily produced. A viable candidate is the intercalating mixed-valence transition metal hexacyanoferrate (MHCF) class of compounds, of which the classic example is Prussian Blue, known for centuries but first reported for its electrochromic properties in 1978.<sup>[28]</sup> MHCFs comprise of repeating units of high-spin transition metals connected to low-spin iron centers via cyanide linkages.<sup>[29]</sup> MHCF systems containing electrochemically active high-spin metals like iron and cobalt exhibit two-electron redox events, while electrochemically inert atoms

like copper and nickel yield a material whose redox state is governed only by the valence of the low-spin iron atom.<sup>[30]</sup> The theoretical capacity of the latter type of MHCs is lower, but their cycling longevity is enhanced due to reduced structure deformation from intercalation,<sup>[30b]</sup> with only a ca. 0.2% isotropic lattice strain reported for NiHCF cycling with sodium ions.<sup>[31]</sup> Prussian Blue analogues have varying selectivities toward alkali metal cations,<sup>[32]</sup> and have been reported to be able to intercalate even divalent ions.<sup>[33]</sup> Due to these useful properties, they have been used in ion exchangers for cesium,<sup>[34]</sup> ion-sensing via catalytic reduction of hydrogen peroxide,<sup>[35]</sup> magnetic applications,<sup>[36]</sup> electrochromic displays,<sup>[37]</sup> and as a large-scale energy storage material.<sup>[30b, 38]</sup> In particular, they are desirable redox-active materials because of their simplicity and safety in inexpensive large-scale synthesis by bulk precipitation,<sup>[30b, 38b]</sup> relatively high redox potential,<sup>[30b]</sup> and generally pH-independent behavior.<sup>[38b, 39]</sup> In terms of separations, these species have been used in electrochemically-switched ion exchange (ESIX) processes to remove alkali metal ions, notably cesium, from aqueous media,<sup>[40]</sup> and have been subsequently investigated as CDI electrodes for desalination.<sup>[41]</sup>

In the current work, an asymmetric electrochemical system was developed and investigated for heterogeneous water treatment in the 10 to 100 mM salt concentration range, which is representative of brackish water,<sup>[24, 27]</sup> wastewater,<sup>[42]</sup> and electrocatalytic process conditions for gas production and valorization.<sup>[43]</sup> Specifically, poly(vinylferrocene) was used as the redox-active anode material to electrosorb anionic species, while copper/nickel metal hexacyanoferrates were used at the cathode to electrochemically intercalate monovalent cations (**Figure 1**). Both of these species are notable for their fast and reversible redox reactions.<sup>[31, 44]</sup> This hybrid polymeric-crystalline scheme was found to have an increased ability to separate inorganic transition metal oxyanions,

suppress solution pH increases, and decrease energetic requirements, compared with a system utilizing an inert water splitting cathode. The potential difference for the electrochemical cell was further adjusted by tuning the redox potential of the MHCF at the cathode via the ratio of its high-spin sites occupied by copper and nickel, resulting in overall potential windows as low as ca. 0.1 V under current densities of ca. 1 A/m<sup>2</sup>. It was found that nickel hexacyanoferrate (NiHCF) offered the most desirable characteristics as a cathode relative to its copper/nickel counterparts due to its high initial extent of oxidation, as well as having a redox potential closest to that of the PVFc anode. The final PVFc//NiHCF pairing resulted in a promising low-energy electrochemically-mediated redox-active alternative for next-generation water treatment.

## 2. Methods

The electrodes used in this work were prepared via a solvent-based film deposition technique. Carbon black (CB) dispersions were made with well-ground redox-active material, conductive CB, and polymer binder. Electrodes were fabricated by drop-casting the dispersions onto conductive Teflon-coated carbon fibers, and removing the solvent to generate a film. This technique was adapted from previously reported non-covalent functionalization methods.<sup>[38b, 44-45]</sup> Conductive poly(vinylferrocene) composites were used as the working anodes. PVFc-CB electrodes were made with 150  $\mu$ L of a dispersion containing 3 mg PVFc, 3 mg CB, and 1 mg poly(vinylidene fluoride) (PVDF) per 1 mL *N,N*-Dimethylformamide (DMF). Conductive copper/nickel hexacyanoferrate ([Cu/Ni]HCF) composites were used as the working cathodes. [Cu/Ni]HCF-CB electrodes were made with 15-20  $\mu$ L of a dispersion containing 100 mg [Cu/Ni]HCF, 10 mg CB, and 10 mg PVDF per 1 mL 1-Methyl-2-pyrrolidinone (NMP). The [Cu/Ni]HCF crystals were synthesized via controlled dropwise addition of precursors, as adapted from previously reported co-precipitation techniques.<sup>[31, 38b, 46]</sup>



Electrochemical separation of the inorganic compounds was carried out using PVFc-CB and CB/NiHCF-CB electrodes containing double the amount of composite material (150  $\mu\text{L}$  and 30  $\mu\text{L}$ , respectively), which was achieved by applying the slurry to both sides of the carbon paper substrate via the same solution casting procedure. These experiments were generally performed with a three-electrode setup at 0.8 V vs Ag/AgCl for 1800 s in 5 mL of solution containing 1 mM adsorbate and 20 mM  $\text{NaClO}_4$ , with stirring under ambient conditions, unless otherwise specified. Electro-desorption experiments were performed in the same way, but at 0 V vs Ag/AgCl in 20 mM  $\text{NaClO}_4$ , unless otherwise specified.

Cyclic voltammetry, electrochemical impedance, open-circuit, and chronocoulometry experiments were carried out with a platinum wire counter electrode, unless otherwise specified.

Further details on preparation methods and characterization can be found in the Supporting Information.

### 3. Results and Discussion

#### 3.1. Material characterization

##### 3.1.1. *[Cu/Ni]HCF crystalline particles*

In this work, the proportions of copper and nickel atoms within the [Cu/Ni]HCF crystal framework were altered by tuning the copper-to-nickel ratio of the feed precursors to yield a mixed crystal solid solution of the form  $\text{Cu}_{1-y}\text{Ni}_y\text{HCF}$  (where  $y$  is the nickel mole fraction), as was achieved through a previously reported method.<sup>[46]</sup> Crystals made with feed precursor ratios of only copper, only nickel, and equimolar copper and nickel are denoted as CuHCF, NiHCF, and CuNiHCF, respectively. The actual copper-to-nickel ratio was determined through inductively-coupled plasma mass

spectrometry (ICP-MS) analysis of the microwave-digested bulk hybrid crystal samples. The synthesized particles were observed to be crystalline with the characteristic face-centered-cubic Prussian Blue structure from measured X-ray diffraction (XRD) patterns (**Figure S1** and **S2**, Supporting Information), and were nano-sized at less than 100 nm as determined by transmission electron microscopy (TEM) imaging (**Figure 2a**). Thermogravimetric analysis (TGA) of the NiHCF sample revealed a 29.9 wt% fraction of both weakly adsorbed and coordinated water within the crystal structure (**Figure S3**, Supporting Information), which corresponds well with literature reports.<sup>[31, 47]</sup> Coupled with combustion elemental analysis (for C/H/N) and inductively-coupled plasma optical emission spectroscopy (ICP-OES) analysis (for K/Ni/Fe), the TGA allowed for the calculation of an overall empirical chemical formula for the synthesized NiHCF:  $K_{0.11}Ni_{1.66}[Fe(CN)_6] \cdot 8.25H_2O$ , with the K contribution coming from the potassium counter-ion of the ferricyanide salt used in the synthesis. Fourier-transform infrared (FTIR) spectra of the NiHCF material confirmed the Prussian blue crystal structure (**Figure S4**, Supporting Information).<sup>[48]</sup> A maximum at  $2167\text{ cm}^{-1}$  arose from the  $\nu(C\equiv N)$  stretching vibration, with a weak shoulder at  $2101\text{ cm}^{-1}$ , matching well with observations from previous studies.<sup>[49]</sup> It is also of note that the wavenumber of the strong cyanide peak was similar to that of the  $Fe(CN)_6^{3-}$  ferricyanide species.<sup>[50]</sup> The presence of coordinated water was also observed through a stretching mode broad band with a maximum at  $3405\text{ cm}^{-1}$ , as well as the  $\delta(H_2O)$  bending mode at  $1610\text{ cm}^{-1}$ .<sup>[51]</sup>

### 3.1.2. PVFc-CB and [Cu/Ni]HCF-CB electrodes

The conductive carbon composite electrodes were characterized to investigate the presence and activity of the redox-active species. XRD patterns of the [Cu/Ni]HCF-CB composite materials showed characteristic peaks of the redox-active [Cu/Ni]HCF components at ca.  $15^\circ$  (111),  $17^\circ$  (200),  $25^\circ$  (220),

35° (400), and 40° (420) (**Figure S5**, Supporting Information). For these Miller indices, a slight peak shift towards lower angles was observed with increasing nickel content, in line with previous literature results.<sup>[46]</sup> These results further suggested that the mixed crystals were not merely mechanical mixtures of CuHCF and NiHCF. X-ray photoelectron spectroscopy (XPS) confirmed the presence of PVFc (3.8 mol% Fe) in PVFc-CB, which corresponds with the theoretically drop-casted amount per electrode of 2.9 mol% Fe, on the basis of the three main elements being C, F, and Fe (**Figure S6a**, Supporting Information). Similarly, NiHCF was identified in NiHCF-CB through the observance of Ni, Fe, and N peaks (**Figure S6b**, Supporting Information), which were not present in the pure CB sample (**Figure S6c**, Supporting Information). TGAs of the pure and composite materials (**Figure S7**, Supporting Information) revealed that the mass remaining of NiHCF-CB was 42.9 wt% of its original value, aligning closely with the expected amount of 47.9 wt% calculated based on the TGA mass losses of its individual components. The PVFc-CB material exhibited improved thermal stability, with 64.2 wt% of the composite material remaining as opposed to the expected 46.8 wt%. Since the TGA of pure PVFc showed virtually no mass left behind (2.5 wt%), this difference may be a result of restricted thermal motion in a nanocomposite material, which can hinder further decomposition and evaporation of decomposed molecule fragments.<sup>[52]</sup> Surface area measurements via nitrogen adsorption using the Brunauer-Emmett-Teller (BET) theory yielded values of 56.4, 31.2 and 45.5 m<sup>2</sup>/g for CB, PVFc-CB, and NiHCF-CB, respectively (**Figure S8**, Supporting Information). The high porosities, as well as the uniform morphology of these nanostructured composites, were also observed through scanning electron microscopy (SEM) imaging (**Figure 2b** and **Figure S9**, Supporting Information).

The conductive network provided by the composites greatly enhanced the utilization of the pure redox-active species. Specifically, a redox-active material-to-carbon black mass ratio of 1:1 for PVFc-CB and 10:1 for NiHCF-CB increased the pseudocapacitive charge response by fifty-fold and twenty-fold, respectively, to yield conductive composites that had similar pseudocapacitances in the range of ca. 125 mF (**Figure S10**, Supporting Information), with charge-transfer resistances of ca. 20  $\Omega$  (**Figure S11**, Supporting Information). The [Cu/Ni]HCF-CB composites exhibited tunable redox potentials, as seen from the leftwards shift of the cyclic voltammograms (CV) towards lower potentials with increasing nickel content (**Figure 2c**).

### 3.2. Electronic properties of the [Cu/Ni]HCF system

#### 3.2.1. Electrochemically-mediated intercalation

MHCF species allow for the intercalation of certain ions into their lattices (**Figure 3a**), and this is reflected in their solution phase redox-active behavior. Specifically, the channel diameter of the open-framework MHCF crystalline structure is correlated with the size of its high-spin atom, however, the lattice constants of most MHCF species are comparable at ca. 10 Å based on the size of the large cyanide ion.<sup>[29c, 30a]</sup> CVs of NiHCF-CB carried out in constant ionic strength 0.1 M nitrate solutions with varying cations illustrated this physical trend, namely, both the oxidation and reduction peaks clearly shifted rightwards to more positive potentials in the presence of ions with smaller hydrated ionic radii (**Figure S12**, Supporting Information). The observed affinity was  $\text{Cs}^+ > \text{Rb}^+ > \text{K}^+ > \text{Na}^+ > \text{Li}^+$ , which matched the trends from other experimental literature studies,<sup>[53]</sup> as well as previously derived relations where the insertion potential scales linearly with and is inversely proportional to the inserted ion's ionic potential.<sup>[54]</sup> This result exemplifies the size-dependent

intercalative nature of the ion sorption mechanism, with the general observation that smaller hydrated ions seem to more easily enter the interstitial pores.<sup>[32b, 32c]</sup>

### 3.2.2. Redox potential

The ionic potential of the high-spin atom within the MHCF structure is also positively correlated with the redox potential of the MHCF material.<sup>[55]</sup> In the [Cu/Ni]HCF system, an increase in the nickel content relative to copper decreased the redox potential (determined from the half potential of the CV peaks) in a linear fashion, affording a total tunable potential range of ca. 0.27 V, with pure CuHCF at ca. 0.71 V vs Ag/AgCl, and pure NiHCF at ca. 0.44 V vs Ag/AgCl (**Figure 3b**). This range of accessible potentials as well as the linearity of the trend was comparable with that of previous studies of other mixed hexacyanoferrates such as [Ni/Pd]HCF,<sup>[56]</sup> [Ni/Fe]HCF,<sup>[57]</sup> and [Cd/Fe]HCF,<sup>[58]</sup> which is of particular note since the electronegativities of copper and nickel are very similar, while a larger difference exists between the other pairs. In general, the dependence of redox potential on the MHCF high-spin atom has been previously explained by the effect of  $\pi$ -backbonding between the low-spin iron and the carbon atom in the cyanide ligand, whereby a high-spin atom with a higher ionic potential weakens the iron-cyanide  $\sigma$  bond and enhances  $\pi$ -backbonding, resulting in a decrease in the energy of the  $t_{2g}$  orbitals and subsequent increase of the redox potential to more positive values.<sup>[29c, 55]</sup>

### 3.2.3. Initial extent of oxidation

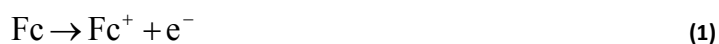
It was observed that changing the fractions of the two metals also affected the incipient oxidation state of the as-made hybrid material, with a higher nickel mole fraction resulting in greater oxidation, as seen by the increased presence of the  $\text{Fe}^{\text{III}}\text{-CN-M}^{\text{II}}$  bond at ca.  $2165\text{ cm}^{-1}$  over the  $\text{Fe}^{\text{II}}\text{-}$

CN-M<sup>II</sup> bond at ca. 2101 cm<sup>-1</sup> (**Figure 3c**) from infrared spectroscopy.<sup>[49, 59]</sup> The mode assignments arise because the decrease in the electronegativity of the low-spin iron heightens the iron-carbon  $\sigma$ -bonding, shifting the wavenumber to higher values.<sup>[29a]</sup> Open-circuit voltage measurements of the as-made [Cu/Ni]HCF-CB electrodes (**Figure S13**, Supporting Information) revealed that their initial oxidation states varied based on the amount of nickel in the [Cu/Ni]HCF crystal structure. In comparison with the peak oxidation and reduction potentials of each [Cu/Ni]HCF-CB electrode from cyclic voltammetry (**Figure 2c**), it was observed that a higher nickel content raised the open-circuit potential closer towards the peak oxidation potential (**Figure 3d**). NiHCF-CB had an open-circuit potential significantly higher than the CV-derived redox potential (ca. 0.58 V as compared to ca. 0.43 vs Ag/AgCl), corroborating the previous observation of a higher extent of initial oxidation in NiHCF. Chronocoulometry experiments at the peak oxidation and reduction potentials of the [Cu/Ni]HCF-CB composite electrodes further supported this, with NiHCF-CB having the highest reduction current and lowest oxidation current in its as-made state (**Figure S14a** and **S14b**, Supporting Information). A possible explanation for this observation may be that the crystals were synthesized in water, as fully oxidized CuHCF has a high redox potential and has previously been observed to be reduced by water.<sup>[33, 60]</sup>

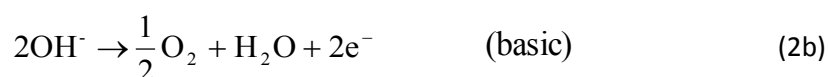
### 3.3. Electrochemical PVFc-CB//[Cu/Ni]HCF-CB system

#### 3.3.1. Faradaic redox equations

The electrochemical system is defined by an anode and cathode for the surface-functionalized heterogeneous Faradaic half-cell reactions (**Figure 1**). During ion adsorption, the anode and cathode undergo oxidation and reduction, respectively. At the anode, the half-cell reaction for the ferrocene (Fc) moieties can be written as a one-electron oxidation to ferrocenium (Fc<sup>+</sup>) (**Equation 1**).<sup>[61]</sup>



The corresponding parasitic side reaction at the anode is water oxidation (**Equation 2a and 2b**):



At the cathode, the general reduction half-cell reaction for the [Cu/Ni]HCF nanoparticles can be expressed as (**Equation 3**):<sup>[30b, 31, 62]</sup>



Where A is the cation intercalated into the [Cu/Ni]HCF crystal structure. The corresponding parasitic side reaction at the cathode is water reduction (**Equation 4a and 4b**):



As can be observed, the insertion reaction consists of two coupled electrochemical processes, namely, an electron transfer step that decreases the low-spin iron oxidation state, and an ion transfer step from the electrolyte into the open structure to maintain charge neutrality (Figure 3a).<sup>[30a]</sup>

### 3.3.2. *Electrochemical performance in aqueous media*

Electrochemical studies were carried out to assess the energetic performance of the Faradaic PVFc-CB//[Cu/Ni]HCF-CB system. Chronopotentiometry experiments showed that increasing the

nickel content within the [Cu/Ni]HCF structure lowered the cathode potential required to sustain the current from anodic oxidation (**Figure 4a**). The anode electrode potentials were consistently at ca. 0.4 V vs Ag/AgCl for PVFc oxidation, and the cathode electrode potentials ranged from ca. 0.45 V to 0.59 V vs Ag/AgCl based on the [Cu/Ni]HCF species used for reduction, corroborating the results from the cyclic voltammetry studies (**Figure 2c**). Thus, in the context of the mixed  $\text{Cu}_{1-y}\text{Ni}_y\text{HCF}$  framework, NiHCF-CB was the most desirable cathode material for the application since it yielded the lowest possible cell potential with PVFc-CB (**Figure 4a**), and started in the most oxidized state as compared to its copper-containing counterparts (**Figure 3c and 3d**), providing more initial capacity for its use in reduction. This attribute is especially noteworthy as it was experimentally observed that the low incipient oxidation of CuHCF-CB rendered it unable to balance the oxidation of PVFc-CB (which is reduced in its initial as-made state) for extended durations when used as a cathode in its as-made state. The redox states of the as-made electrodes of [Cu/Ni]HCF-CB and PVFc-CB were studied separately through chronocoulometry experiments (**Figure S14**, Supporting Information).

Further electrochemical tests using the NiHCF-CB cathode exemplified its favorable energetics. Chronoamperometry (**Figure 4b**) and chronopotentiometry experiments (**Figure 4c and S15**, Supporting Information) revealed that the PVFc-CB//NiHCF-CB system only required small voltage swings (ca. 0.1 V at ca.  $1 \text{ A/m}^2$ ) as compared with systems using conventional cathode materials like carbon black and platinum (ca. 0.77 V and 1.24 V, respectively, at ca.  $1 \text{ A/m}^2$ ). Cyclic voltammetry performed with a two-electrode setup across the water stability window (-1 to 1 V) showed successful activation of the ferrocene moieties only when NiHCF-CB was used as the counter electrode, since potentials beyond those of water splitting were required if CB was used instead (**Figure S16**, Supporting Information). As expected, when the Faradaic charge of the heterogeneous



redox-active species was depleted, the cell potential increased to that of a non-redox CB//CB system as the electrodes began to mediate water splitting to sustain the cell current (**Figure 4d**). The half-cell reactions occurring at the anode and cathode were determined by tracking the individual potentials of each electrode (**Figure S17**, Supporting Information). The occurrence of the parasitic water reduction reaction at CB decreased the cathode potential during reduction, raising the total energy required to sustain the oxidation of the PVFc-CB anode. In contrast, the NiHCF-CB cathode suppressed pH increases in the solution by re-directing electrons to facilitate cation intercalation (**Figure 4b**). This provided further benefit as it has previously been shown that basic solutions significantly hinder the ability of PVFc to adsorb anions.<sup>[21]</sup>

The operation of the asymmetric Faradaic cell was also shown to be sustainable through conditioning tests via continuous cycling (**Figure S18a**, Supporting Information). Chronocoulometry experiments carried out on separate PVFc-CB and NiHCF-CB electrodes also showed their individual retention of electrochemical capacity after repeated cycles (**Figure S18b** and **S18c**, Supporting Information). The solutions before and after these cycling tests were microwave-digested and analyzed with ICP-MS to quantify any leaching of redox-active material. The results revealed only minimal increases in the solution iron concentration, corresponding to < 1% leachate for PVFc-CB and < 2% for NiHCF-CB (determined from the theoretical mass of redox-active material on each electrode based on the feed amount in the electrode dispersions).

### 3.4. Electrochemical Separation of Inorganic Species

#### 3.4.1. Heavy Metal Oxyanions (HMOA)

Ferrocenium has previously been found to exhibit high uptake capacities, selectivities, and reversible electrosorption/desorption behavior for toxic transition metals in the form of oxyanions,

namely, chromates and arsenates.<sup>[18a]</sup> Applying the PVFc-CB//CB system for electrosorption in a solution of 1 mM  $\text{Na}_2\text{Cr}_2\text{O}_7$  and 20 mM  $\text{NaClO}_4$  yielded a chromium uptake capacity of ca. 31 mg/g PVFc-CB, which matched very closely with previously reported separation results using a PVFc-carbon nanotube composite under the same conditions (**Figure 5a**). Remarkably, by changing the cathode electrode to NiHCF-CB, the adsorption capacity almost doubled to ca. 58 mg/g PVFc-CB. In addition, PVFc-CB was also observed to have affinity for other HMOAs such as the tetrahedral  $\text{MoO}_4^{2-}$  and the polymeric  $\text{VO}_3^-$ , with similar increases in adsorption capacity observed when NiHCF-CB was used as the cathode (**Figure 5a**).

This adsorption enhancement from the asymmetric PVFc-CB//NiHCF-CB system is likely due to the intercalation of sodium ions into the cathode further promoting anion uptake at the anode to maintain electroneutrality. High-resolution XPS experiments conducted on NiHCF-CB electrodes after electrosorption confirmed that the intercalation of sodium ions into the crystalline framework is electrochemically-mediated. Previous work in the literature has also shown that the lattice parameter of NiHCF increases with sodium intercalation.<sup>[31]</sup> After applying a cell current, a peak corresponding to the Na 1s transition was observed, whereas under open-circuit voltage (i.e. zero current), this peak was not observed (**Figure 5b**). The surface water on these samples was removed prior to evaporation at ambient conditions, and as such, the appearance of a small Na 1s signal on a charged CB electrode suggests the presence of electrosorbed sodium on the surface. In addition, high-resolution XPS experiments on electrodes after molybdate adsorption with both PVFc-CB//CB and PVFc-CB//NiHCF-CB showed that the magnification of the Mo 3d peak signal at the PVFc-CB anode coincides with an increase in the Na 1s peak signal at the cathode arising from the ability of NiHCF-CB for sodium intercalation (**Figure S19a**, Supporting Information), corroborating the

increases observed from solution-phase quantification studies (Figure 5a). This enhanced anion adsorption from cation intercalation also suggests that the process selectively favors molybdate removal over perchlorate, as the intensities of the Cl 2p signals on the PVFc-CB are comparable over both cathode configurations, with similar PVFc-CB loading amounts on each electrode based on Fe 2p peak intensities (**Figure S19b** and **S19c**, Supporting Information).

To further assess adsorption performance, the PVFc-CB//NiHCF-CB system was operated in the simultaneous presence of  $\text{Cr}_2\text{O}_7^{2-}$  (100 ppb Cr, as per the United States Environmental Protection Agency (EPA) drinking water standard<sup>[63]</sup>),  $\text{MoO}_4^{2-}$  (80 ppb Mo, as per the EPA Health Advisory level for children's drinking water on a 1-day and 10-day basis<sup>[64]</sup>), and  $\text{VO}_3^-$  (100 ppb), at sub-ppm levels reflective of regulation limits. The PVFc-CB electrodes effectively removed significant amounts of the HMOAs ( $\geq 50\%$ ), with the use of the NiHCF-CB counter electrode once again boosting the electrosorption capacity for all species, to an almost 100% recovery of vanadium (**Figure 5c**).

The energy requirements for the electrochemical separations were assessed by performing chronoamperometry in 20 mM  $\text{NaClO}_4$  at adsorption and desorption potentials of 0.8 V and 0 V vs Ag/AgCl, respectively (**Figure 5d** and **S20a**, Supporting Information). When the NiHCF-CB cathode was used over the CB cathode, there was a significant 75.8% and 70.3% reduction in the amount of energy required to maintain the PVFc-CB anode at its adsorption and desorption potentials, respectively. This can be attributed to two main events, namely, the lowering of the magnitude of the cathode reduction potential relative to those of the water splitting side reactions, which reduces the average cell potential,  $E_{\text{cell,avg}}$ , and the prevention of water splitting side reactions, which lowers the total charge passed,  $Q_{\text{total}}$ . These two variables form the total work required to operate the cell,  $W_{\text{cell}}$  (**Equation 5**):

This article is protected by copyright. All rights reserved.

$$W_{\text{cell}} \approx E_{\text{cell,avg}} Q_{\text{total}} \quad (5)$$

Breaking down the energy requirement values in terms of these two values (**Equation S2** and **S3**), it was observed that during adsorption, both  $E_{\text{cell,avg}}$  and  $Q_{\text{total}}$  decreased by 51.2% and 52.3%, respectively, with the use of NiHCF-CB over CB, whereas during desorption,  $E_{\text{cell,avg}}$  decreased by 65.8% while  $Q_{\text{total}}$  remained roughly the same with only a 6.8% decrease (**Figure S20b**, Supporting Information). This suggests that during adsorption, both events contribute equally to the four-fold reduction in energy, whereas during desorption, water splitting side reactions are minimal.

### 3.4.2. Phosphomolybdate

Another class of ionic transition metal complexes is the polyoxometalate (POM), which is a broad grouping of inorganic metal-oxygen cluster anions. A classic example is phosphomolybdic acid ( $\text{H}_3\text{PMo}_{12}\text{O}_{40}$ ), a heteropolyanion with the archetypal Keggin ion structure. Heteropolyacids find application in a plethora of different areas such as oxidative catalysis due to their redox and acidic properties,<sup>[65]</sup> and are applied in industrial homogeneous processes such as isopropyl alcohol production from propene.<sup>[65b, 66]</sup> These techniques are often highly selective (ca. 99% in the case of propene hydrolysis<sup>[66]</sup>), but suffer from difficulties in the separation of the reaction product from the catalyst, leading to catalyst loss or degradation.<sup>[67]</sup> It follows that electrochemically-mediated processes may prove to be useful plug-and-play techniques for catalyst recovery in their original state.

Applying different electrode configurations to a solution of 100  $\mu\text{M}$   $\text{H}_3\text{PMo}_{12}\text{O}_{40}$  and 20 mM  $\text{NaClO}_4$  confirmed that the phosphomolybdate adsorption was electrochemically-mediated by the ferrocene moieties (**Figure 6a**). Interestingly, both PVFc-CB//CB and PVFc-CB//NiHCF-CB yielded comparable electrosorption capacities of ca. 93 and 85 mg Mo/g PVFc-CB, respectively, in stark

contrast to the heavy metal oxyanion separations, which produced marked increases in uptake when a NiHCF-CB cathode was used. This may result from the fact that the counter-ion of the phosphomolybdate ion is a proton (rather than a sodium ion), which is less thermodynamically favored to be intercalated into the NiHCF structure compared to potassium and sodium ions.<sup>[68]</sup> This was supported by the appearance of the Na 1s peak at the NiHCF-CB electrode from XPS measurements (**Figure 6b**), as well as the separate observation that the pH of a solution of 1 mM  $\text{H}_3\text{PMo}_{12}\text{O}_{40}$  and 20 mM  $\text{NaClO}_4$  did not increase from its initial value after electrosorption with PVFc-CB//NiHCF-CB (**Figure S21**, Supporting Information). The suppression of pH increases in the solution with NiHCF-CB is especially pertinent in this application as phosphomolybdate ions begin to degrade even in weakly acidic environments.<sup>[69]</sup> Reversibility of the electrochemical process was also seen through the decreases in intensity of the Mo 3d and Cl 2p signals for the phosphomolybdate (**Figure 6b**) and perchlorate (**Figure S22a**, Supporting Information) ions after electro-desorption. The shift in the Fe 2p peaks of the PVFc-CB electrode back to lower binding energies matching those of an unoxidized control PVFc-CB electrode also exemplified the electrochemically-mediated nature of the desorption process (**Figure S22b**, Supporting Information).

The PVFc-CB//CB system was observed to yield an undesirable effect during electrosorption, namely, the color of the solution quickly changed from almost colorless to blue via the following reduction reaction, with electrons supplied from the CB cathode (**Equation 6**).<sup>[70]</sup>



Fortunately, by using NiHCF-CB as a sink for the electrons, near complete suppression of phosphomolybdic acid reduction to the molybdenum blue species was observed through visual inspection and ultraviolet-visible (UV-Vis) spectroscopy of the resulting supernatant (**Figure S23** and

**S24**, Supporting Information). To complement the solution phase results, the direct generation of the reduced molybdenum blue species was also analyzed using high-resolution XPS on cathode electrodes following electrosorption in 1 mM  $\text{H}_3\text{PMo}_{12}\text{O}_{40}$  and 20 mM  $\text{NaClO}_4$ . After Gaussian peak deconvolution of the Mo 3d spectra, the clear presence of the Mo(V)  $3d_{3/2}$  and  $3d_{5/2}$  peaks was detected on the CB cathode (**Figure 6c**). Conversely, these Mo(V) peaks were present only in small amounts on the NiHCF-CB electrode (**Figure 6d**). In both cases, observed binding energies were similar to those reported in the literature.<sup>[71]</sup> It should be noted that even though the bulk of the solution phase underwent the reduction reaction when CB was used as a cathode, the adsorbed phosphomolybdate at the PVFc-CB anode was mostly oxidized regardless of the cathode used (**Figure S25**, Supporting Information). Lastly, while the reduction of phosphomolybdic acid to molybdenum blue is reversible,<sup>[72]</sup> other POMs such as silicotungstic acid ( $\text{H}_4\text{SiW}_{12}\text{O}_{40}$ ) can irreversibly convert to heteropolybrown species at redox potentials as moderate as -0.72 V vs Ag/AgCl,<sup>[73]</sup> highlighting once again the benefit of a heterogeneously functionalized cathode with high redox potential like NiHCF-CB.

#### 4. Conclusions

A new dual-redox asymmetric set-up making use of the complementary oxidation and reduction properties of a metallopolymer at the anode and a transition metal hexacyanoferrate at the cathode has been formulated for the purpose for performing electrochemically-mediated aqueous separations with greater energy efficiency and enhanced adsorption. Through judicious selection and tuning of the electronic properties of the cathode material, the electrochemical operation window of the overall cell can be reduced to ca. 0.1 V at 1 A/m<sup>2</sup>, almost an order of magnitude lower voltage than state-of-the-art capacitive deionization and electrosorption materials. The facile

kinetics of the two iron-mediated redox-couples allow for reversible in-tandem separation of both anions and monovalent cations. By switching out the commonly used inert electric double layer charging material at the cathode with a Faradaic species, multiple operational benefits arise. Specifically, the electrochemical intercalation behavior of transition metal hexacyanoferrates promotes anionic adsorption at the anode, as well as diverting electrons away from water reduction. Shifting the cathodic half-cell reaction away from water splitting also subdues any increases in solution pH, preventing the formation of nucleophilic hydroxide species from fouling the anode and reducing separation performance. The framework has been successfully tested in representative salinity conditions with environmental contaminants such as heavy metal oxyanions, as well as catalytic redox-active species such as heteropolyacids. Using the functionalized cathode, the recovery of the latter class of materials can also be done without affecting the oxidation state of the bulk material, thus avoiding the need for post-processing treatment.

The power of these electrochemical systems lies in their inherent compact design, process adjustability, and precisely managed reactions. Electrochemical properties can be changed to imbibe highly selective molecular recognition capability, as well as alter operating windows for different conditions. These concepts open a window to the bountiful opportunities of applying asymmetric Faradaic systems to fields such as ion-sensing, desalination, electrocatalysis, and energy storage. Specifically, dual-redox systems like the one illustrated in this study bridge the gap by transferring the benefits of electrochemistry to liquid-phase separation, thus showing high promise for the development of next-generation water purification techniques.

#### **Supporting Information**

Supporting Information is available from the Wiley Online Library or from the author.

## 5. Acknowledgements

This work was supported by ExxonMobil Corp. and a Massachusetts Institute of Technology Abdul Latif Jameel World Water and Food Security Lab (J-WAFS) seed grant. K-J. T. holds a Natural Sciences and Engineering Research Council of Canada (NSERC) postgraduate doctoral scholarship (PGS D).

This work made use of the Materials Research Science and Engineering Centers (MRSEC) Shared Experimental Facilities at the Massachusetts Institute of Technology (supported by the National Science Foundation under award number DMR 1419807), the Center for Environmental Health Sciences at the Massachusetts Institute of Technology (supported by the National Institute of Environmental Health Sciences, National Institutes of Health under core center grant P30-ES002109), the Institute for Soldier Nanotechnologies (ISN) at the Massachusetts Institute of Technology, as well as the Center for Nanoscale Systems (CNS) at Harvard University (supported by the National Science Foundation under award number 1541959).

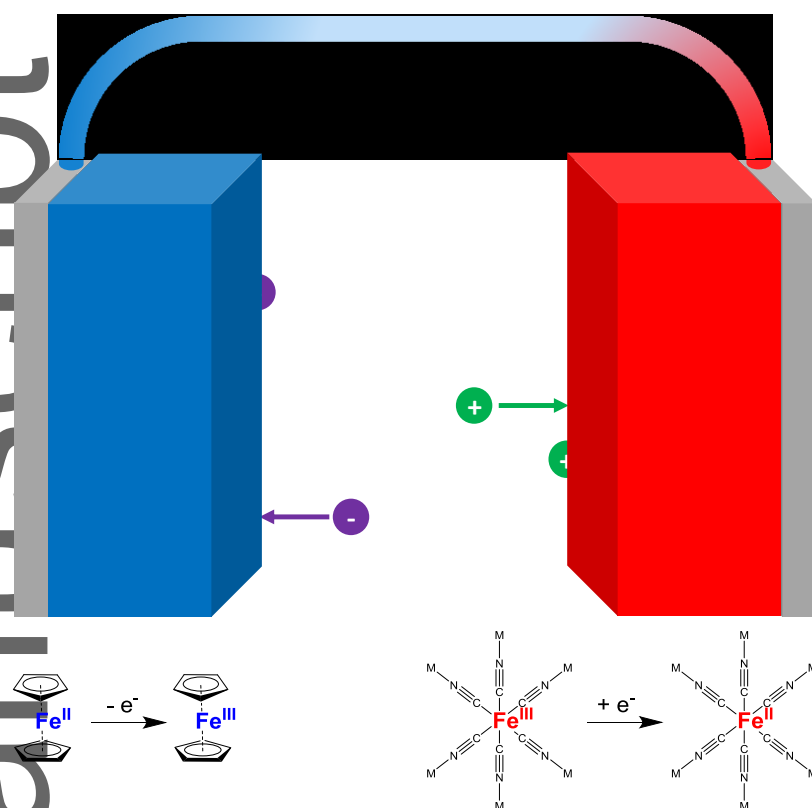
The authors gratefully acknowledge Dr. Yayuan Liu and Dr. Katherine Phillips for their help in performing and discussing XPS measurements. The authors would also like to thank Miao Wang for assistance with pH and XRD measurements, Eliza Khokhar and André Tschöpe for help with electrode fabrication, Liruonong Zhang for help with initial electrode development and testing, and Dr. Lev Bromberg for insightful discussions.

Received: ((will be filled in by the editorial staff))

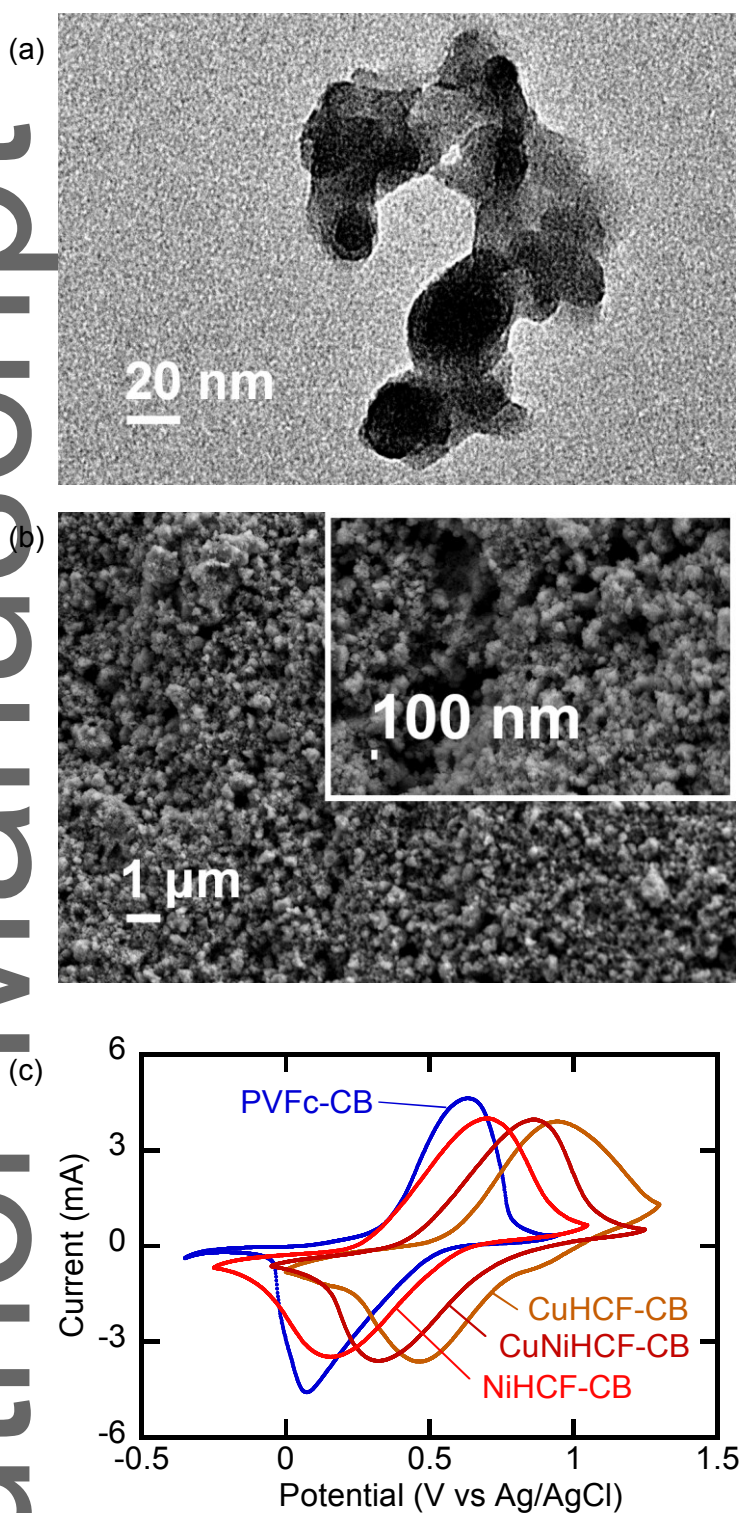
Revised: ((will be filled in by the editorial staff))

Published online: ((will be filled in by the editorial staff))

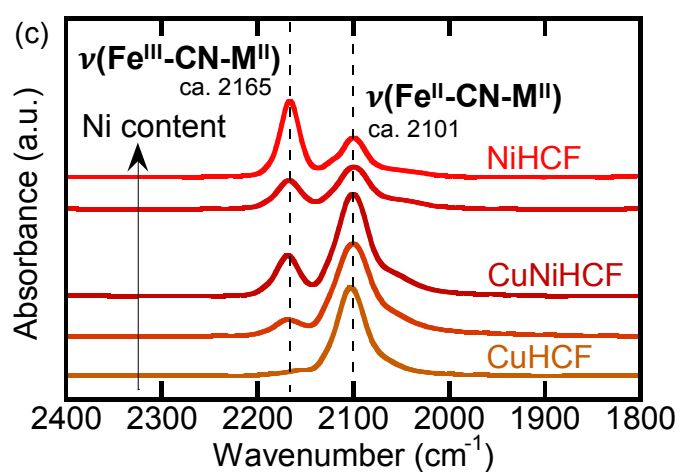
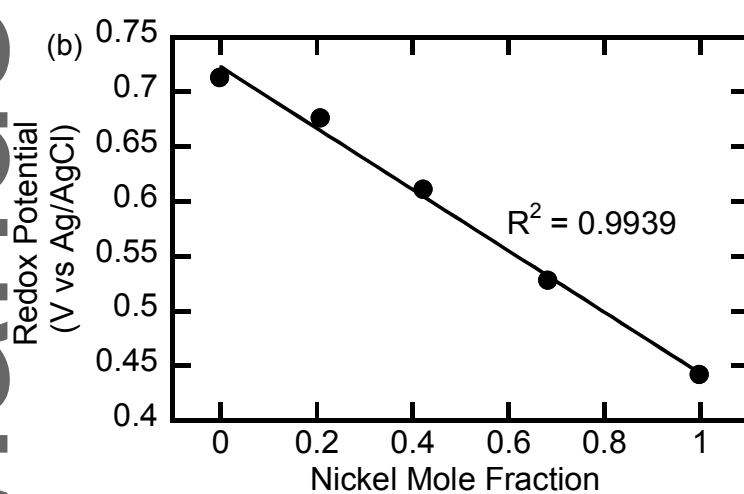
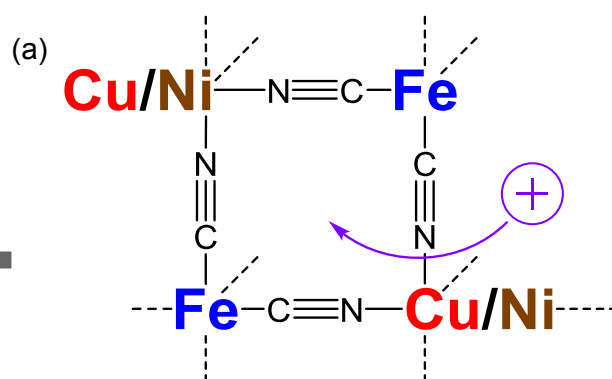


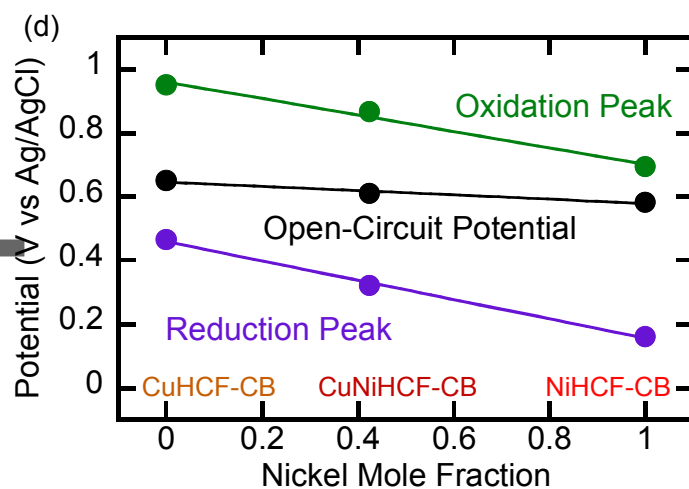


**Figure 1.** Schematic of the asymmetric Faradaic cell configuration. A metallopolymer containing ferrocene moieties at the anode (blue) oxidizes to its cationic state to electrosorb anions, and a crystal containing hexacyanoferrate species at the cathode (red) balances the charge through reduction and cation intercalation into its host framework.

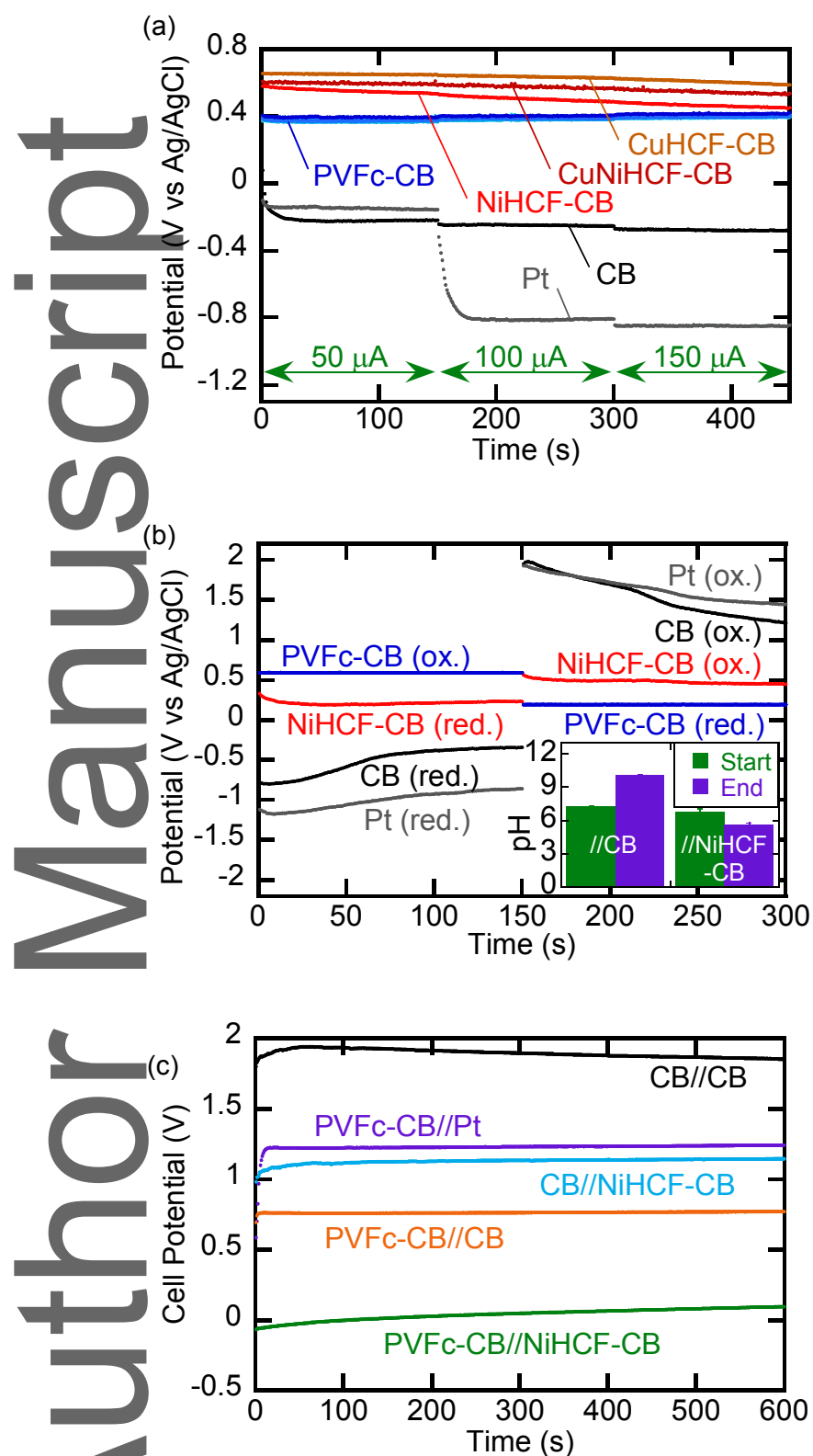


**Figure 2.** (a) TEM image of NiHCF nanoparticles. (b) SEM images of NiHCF-CB. (c) Representative CVs of PVFc-CB and [Cu/Ni]HCF-CB electrodes at 0.01 V/s in 0.1 M KClO<sub>4</sub>.

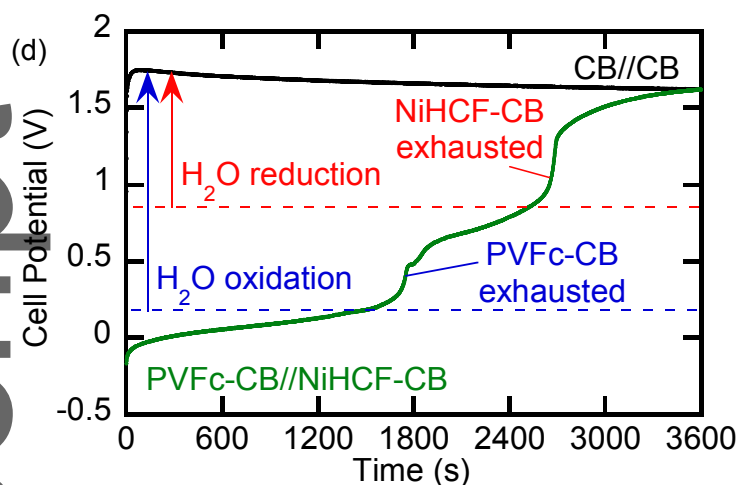




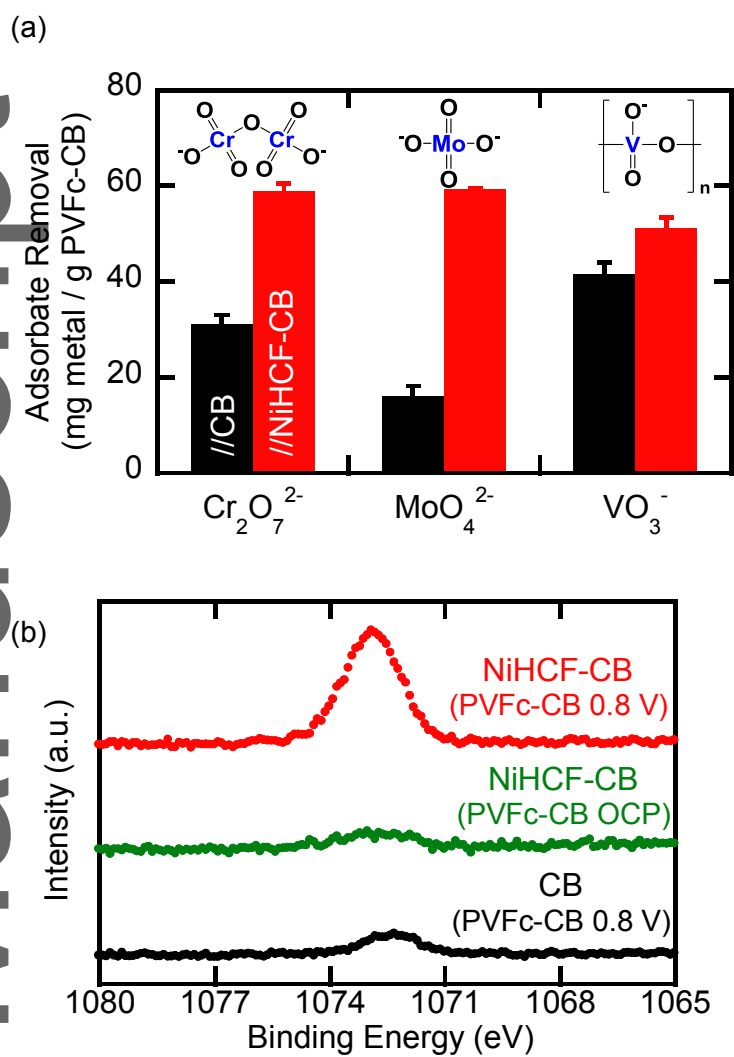
**Figure 3.** (a) Schematic depicting the crystalline structure of [Cu/Ni]HCF and cation intercalation behavior. (b) Variation of  $\text{Cu}_{1-y}\text{Ni}_y\text{HCF}$  redox potential with nickel mole fraction  $y$ , determined from CVs at 0.01 V/s in 0.1 M  $\text{KClO}_4$ . (c) FTIR spectra showing the variation in incipient oxidation state of the as-made  $\text{Cu}_{1-y}\text{Ni}_y\text{HCF}$  material with nickel mole fraction  $y$ . (d) Open-circuit potentials of [Cu/Ni]HCF-CB electrodes in 0.1 M  $\text{KClO}_4$  relative to their corresponding peak oxidation and reduction potentials (determined from CVs at 0.01 V/s in 0.1 M  $\text{KClO}_4$ ).

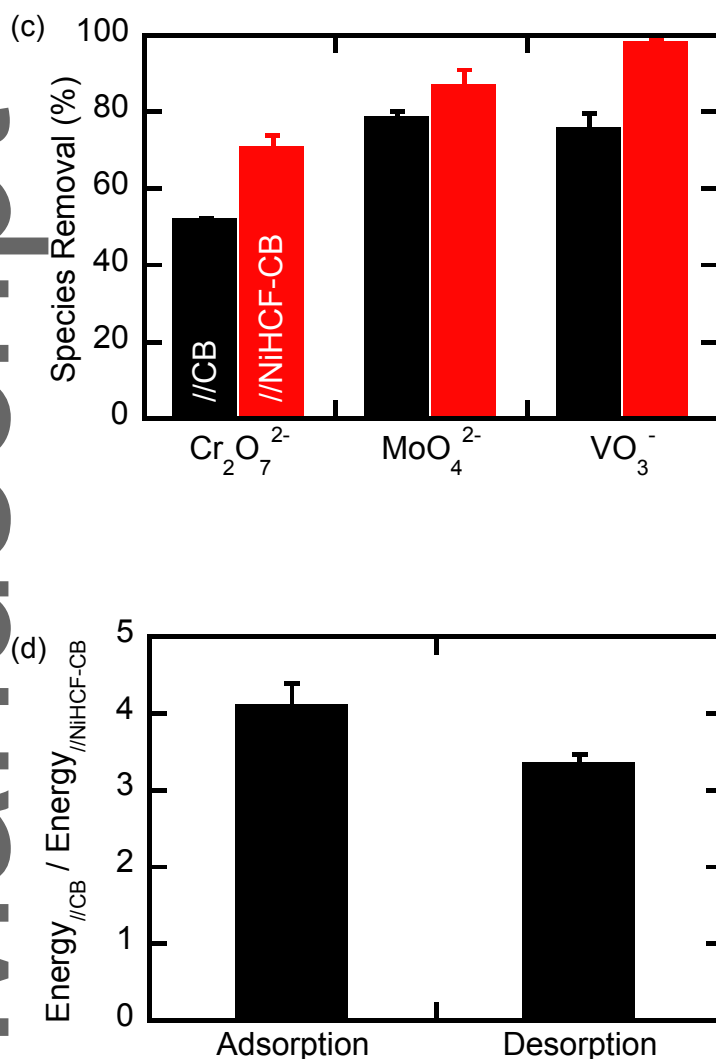


This article is protected by copyright. All rights reserved.



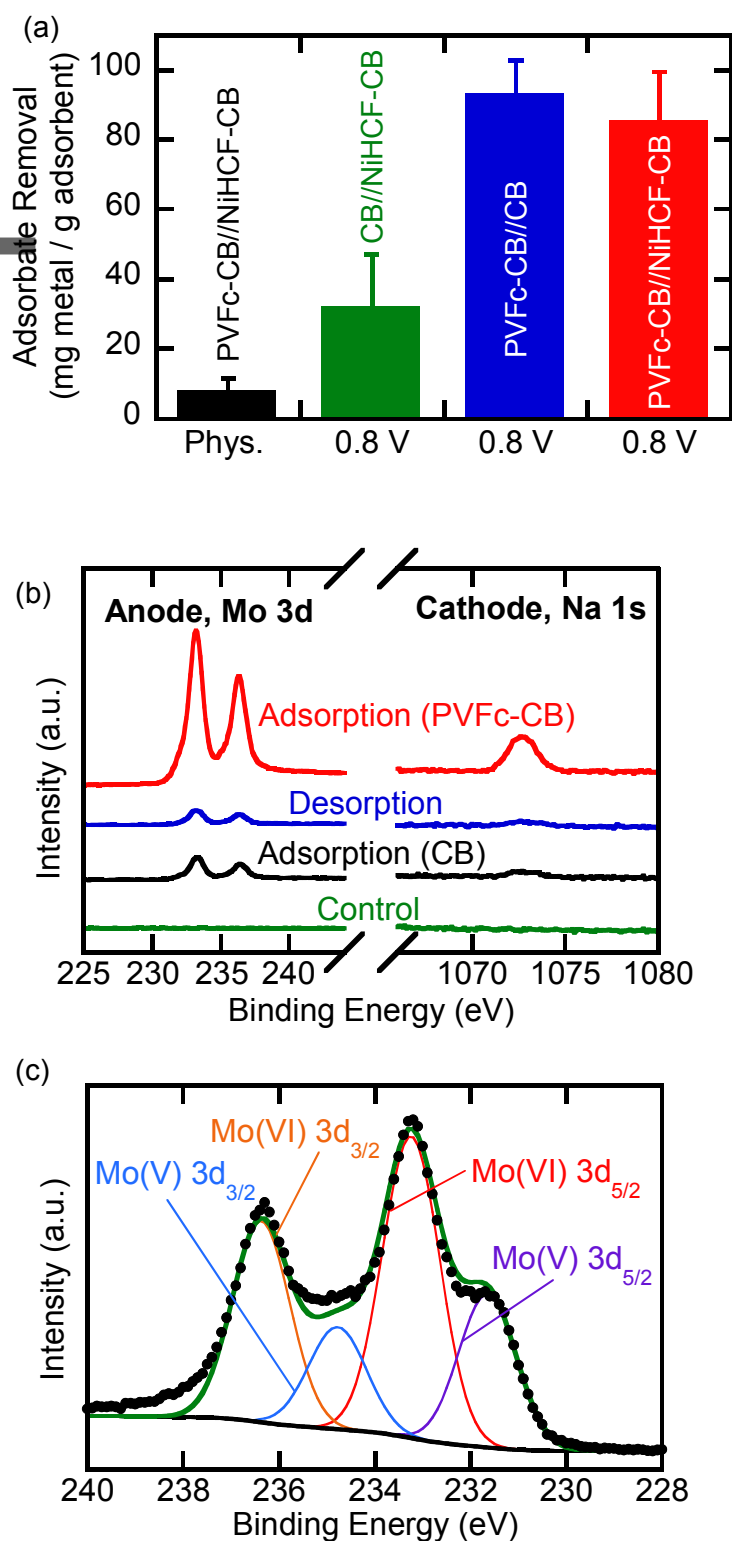
**Figure 4.** (a) Two-electrode chronopotentiometry experiments for a PVFc-CB anode and varying cathode materials at ca. 50  $\mu\text{A}$  (ca. 0.5  $\text{A}/\text{m}^2$ ), 100  $\mu\text{A}$  (ca. 1  $\text{A}/\text{m}^2$ ), and 150  $\mu\text{A}$  (ca. 1.5  $\text{A}/\text{m}^2$ ) in 0.1 M  $\text{KClO}_4$ , with a separate Ag/AgCl reference electrode to track both electrode potentials. (b) Three-electrode chronoamperometry experiments for the oxidation and subsequent reduction of PVFc-CB at ca. 0.6 V and 0.2 V vs Ag/AgCl, respectively, in 0.1 M  $\text{NaClO}_4$ , with the corresponding parasitic (CB) and non-parasitic (NiHCF-CB) counter electrode potentials required to support the anodic electrochemical process. Inset: Solution pH changes incurred after 600 s with CB and NiHCF-CB counter electrodes for the oxidation of PVFc-CB at 0.6 V vs Ag/AgCl in 0.1 M  $\text{NaClO}_4$ . (c) Two-electrode chronopotentiometry experiments at 100  $\mu\text{A}$  (ca. 1  $\text{A}/\text{m}^2$ ) in 0.1 M  $\text{NaClO}_4$ , illustrating the total cell potential required to sustain the positive current for various anode//cathode combinations. (d) Two-electrode chronopotentiometry experiments for the PVFc-CB//NiHCF-CB system at ca. 100  $\mu\text{A}$  (ca. 1  $\text{A}/\text{m}^2$ ) in 0.1 M  $\text{NaClO}_4$ , illustrating the increase in cell potential when the PVFc-CB electrode depletes its charge (blue), followed by the NiHCF-CB electrode (red). Changes in cell potential were determined with a separate Ag/AgCl reference electrode to track both electrode potentials.





**Figure 5.** (a) Adsorbate removal with PVFc-CB//CB and PVFc-CB//NiHCF-CB in different HMOA solutions, after electrosorption for 1800 s at 0.8 V vs Ag/AgCl in 1 mM analyte and 20 mM NaClO<sub>4</sub>. (b) High-resolution XPS Na 1s spectra of CB and NiHCF-CB electrodes after their corresponding PVFc-CB anodes were subject to 0.8 V vs Ag/AgCl (black and red) and open-circuit voltage (green) for 1800 s in 20 mM NaClO<sub>4</sub>. (c) Adsorbate removal with PVFc-CB//CB and PVFc-CB//NiHCF-CB in a mixture of HMOA species after electrosorption for 7200 s at 0.8 V vs Ag/AgCl in relevant regulatory concentrations (ppb level) and 20 mM NaClO<sub>4</sub>. (d) Ratios of the energies expended by the PVFc-CB//CB and PVFc-CB//NiHCF-CB configurations for the PVFc-CB adsorption step (ca. 0.8 V vs Ag/AgCl), and the subsequent desorption step (ca. 0 V vs Ag/AgCl), after 1800 s for each step in 20 mM NaClO<sub>4</sub>.





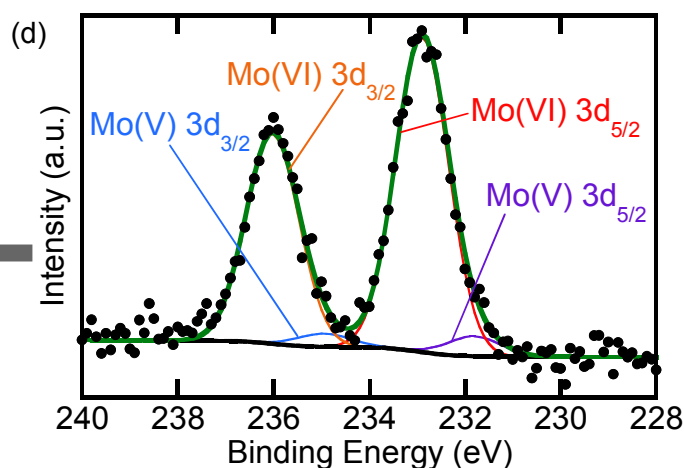


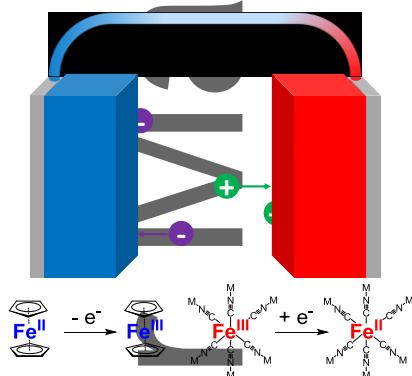
**Figure 6.** (a) Adsorbate recovery amounts using different electrode configurations and electrochemical potentials after 1800 s in 100  $\mu\text{M}$   $\text{H}_3\text{PMo}_{12}\text{O}_{40}$  and 20 mM  $\text{NaClO}_4$ . (b) High-resolution XPS Mo 3d and Na 1s spectra of an as-made PVFc-CB electrode (control), and anodes in the CB//NiHCF-CB and PVFc-CB//NiHCF-CB configurations after electroadsorption for 1800 s at 0.8 V vs Ag/AgCl in 1 mM  $\text{H}_3\text{PMo}_{12}\text{O}_{40}$  and 20 mM  $\text{NaClO}_4$ , or electro-desorption (PVFc-CB//NiHCF-CB) for 5400 s at 0 V vs Ag/AgCl in 20 mM  $\text{NaClO}_4$  (new electrodes used in each case). (c) De-convoluted high-resolution XPS Mo 3d spectra for the phosphomolybdic acid species at the CB cathode after electroadsorption for 1800 s at 0.8 V vs Ag/AgCl in 1 mM  $\text{H}_3\text{PMo}_{12}\text{O}_{40}$  and 20 mM  $\text{NaClO}_4$  with the PVFc-CB//CB configuration. (d) De-convoluted high-resolution XPS Mo 3d spectra for the phosphomolybdic acid species at the NiHCF-CB cathode after electroadsorption for 1800 s at 0.8 V vs Ag/AgCl in 1 mM  $\text{H}_3\text{PMo}_{12}\text{O}_{40}$  and 20 mM  $\text{NaClO}_4$  with the PVFc-CB//NiHCF-CB configuration.

## Electrochemical separations

K.-J. Tan, X. Su, T. A. Hatton

An asymmetric iron-based redox-active system for electrochemical separation of ions in aqueous media

**Redox-active materials for electrochemically-mediated ion removal** are emerging as a potential next-generation technology for water remediation. An asymmetric framework combining an anodic metallopolymer and cathodic hexacyanoferrate crystal for the first time exhibits enhanced adsorption capability for toxic heavy metal oxyanions and polyoxometalate species, with operating windows that can be tuned to as low as ca. 0.1 V at 1 A/m<sup>2</sup>.



## References

- [1] a) P. T. Anastas, J. B. Zimmerman, *Environmental Science & Technology* **2003**, 37, 94A; b) D. S. Sholl, R. P. Lively, *Nature* **2016**, 532, 435.
- [2] M. M. Mekonnen, A. Y. Hoekstra, *Science Advances* **2016**, 2, e1500323.
- [3] a) W. A. Jury, H. Vaux, *Proceedings of the National Academy of Sciences of the United States of America* **2005**, 102, 15715; b) M. A. Shannon, P. W. Bohn, M. Elimelech, J. G. Georgiadis, B. J. Mariñas, A. M. Mayes, *Nature* **2008**, 452, 301.
- [4] J. Radjenovic, D. L. Sedlak, *Environmental Science & Technology* **2015**, 49, 11292.
- [5] F. Fu, Q. Wang, *Journal of Environmental Management* **2011**, 92, 407.
- [6] I. Sirés, E. Brillas, *Environment International* **2012**, 40, 212.
- [7] X. Su, L. Bromberg, K.-J. Tan, T. F. Jamison, L. P. Padhye, T. A. Hatton, *Environmental Science & Technology Letters* **2017**, 4, 161.
- [8] a) X. T. Le, P. Viel, P. Jégou, A. Sorin, S. Palacin, *Separation and Purification Technology* **2009**, 69, 135; b) V. Pascal, D. Laetitia, L. Joël, S. Marc, P. Serge, *Applied Surface Science* **2007**, 253, 3263.
- [9] a) J. W. Blair, G. W. Murphy, in *Saline Water Conversion*, Vol. 27, American Chemical Society, USA **1960**, Ch. 20, p. 206; b) M. E. Suss, S. Porada, X. Sun, P. M. Biesheuvel, J. Yoon, V. Presser, *Energy & Environmental Science* **2015**, 8, 2296.
- [10] a) B. E. Conway, *Journal of The Electrochemical Society* **1991**, 138, 1539; b) F. He, P. M. Biesheuvel, M. Z. Bazant, T. A. Hatton, *Water Research* **2018**, 132, 282.
- [11] a) B. E. Conway, V. Birss, J. Wojtowicz, *Journal of Power Sources* **1997**, 66, 1; b) P. Novák, K. Müller, K. S. V. Santhanam, O. Haas, *Chemical Reviews* **1997**, 97, 207; c) N. Nitta, F. Wu, J. T. Lee, G. Yushin, *Materials Today* **2015**, 18, 252; d) D. S. Achilleos, T. A. Hatton, *Journal of Colloid and Interface Science* **2015**, 447, 282.
- [12] a) X. Su, T. A. Hatton, *Advances in Colloid and Interface Science* **2017**, 244, 6; b) X. Su, T. A. Hatton, *Physical Chemistry Chemical Physics* **2017**, 19, 23570.
- [13] a) E. Bakker, M. Telting-Diaz, *Analytical Chemistry* **2002**, 74, 2781; b) C. Zhu, G. Yang, H. Li, D. Du, Y. Lin, *Analytical Chemistry* **2015**, 87, 230.

- [14] a) T. J. Kealy, P. L. Pauson, *Nature* **1951**, 168, 1039; b) G. Wilkinson, M. Rosenblum, M. C. Whiting, R. B. Woodward, *Journal of the American Chemical Society* **1952**, 74, 2125; c) E. O. Fischer, W. Pfab, *Zeitschrift für Naturforschung B* **1952**, 7, 377; d) J. D. Dunitz, L. E. Orgel, A. Rich, *Acta Crystallographica* **1956**, 9, 373.
- [15] F. S. Arimoto, A. C. Haven, *Journal of the American Chemical Society* **1955**, 77, 6295.
- [16] a) W. S. Schlindwein, A. Kavvada, R. J. Latham, R. G. Linford, *Polymer International* **2000**, 49, 953; b) G. Inzelt, J. Bácskai, *Electrochimica Acta* **1992**, 37, 647; c) H. Gülce, H. Özyörük, A. Yıldız, *Electroanalysis* **1995**, 7, 178; d) I. Jureviciute, S. Bruckenstein, A. R. Hillman, *Journal of Electroanalytical Chemistry* **2000**, 488, 73; e) C. Barbero, M. C. Miras, E. J. Calvo, R. Kötz, O. Haas, *Langmuir* **2002**, 18, 2756.
- [17] a) X. Su, H. J. Kulik, T. F. Jamison, T. A. Hatton, *Advanced Functional Materials* **2016**, 26, 3394; b) D. S. Achilleos, T. A. Hatton, *ACS Applied Materials & Interfaces* **2016**, 8, 32743.
- [18] a) X. Su, A. Kushima, C. Halliday, J. Zhou, J. Li, T. A. Hatton, *Nature Communications* **2018**, 9, 4701; b) K. Kim, S. Cotty, J. Elbert, R. Chen, C.-H. Hou, X. Su, *Advanced Materials* **2019**, 1906877.
- [19] M. Balasubramanian, M. T. Giacomini, H. S. Lee, J. McBreen, J. H. Sukanto, *Journal of The Electrochemical Society* **2002**, 149, D137.
- [20] X. Su, J. Hübner, M. J. Kauke, L. Dalbosco, J. Thomas, C. C. Gonzalez, E. Zhu, M. Franzreb, T. F. Jamison, T. A. Hatton, *Chemistry of Materials* **2017**, 29, 5702.
- [21] X. Su, K.-J. Tan, J. Elbert, C. Rüttiger, M. Gallei, T. F. Jamison, T. A. Hatton, *Energy & Environmental Science* **2017**, 10, 1272.
- [22] a) Y. Luo, W. Guo, H. H. Ngo, L. D. Nghiem, F. I. Hai, J. Zhang, S. Liang, X. C. Wang, *Science of The Total Environment* **2014**, 473-474, 619; b) B. Petrie, R. Barden, B. Kasprzyk-Hordern, *Water Research* **2015**, 72, 3; c) Y. Yang, Y. S. Ok, K.-H. Kim, E. E. Kwon, Y. F. Tsang, *Science of The Total Environment* **2017**, 596-597, 303.
- [23] a) H. S. Kim, Y. J. Kim, Y. R. Seo, *J Cancer Prev* **2015**, 20, 232; b) P. B. Tchounwou, C. G. Yedjou, A. K. Patlolla, D. J. Sutton, *Exp Suppl* **2012**, 101, 133.
- [24] S. Porada, R. Zhao, A. van der Wal, V. Presser, P. M. Biesheuvel, *Progress in Materials Science* **2013**, 58, 1388.
- [25] M. Sathe, L. Yu, Y. Mo, X. Zeng, *Journal of The Electrochemical Society* **2005**, 152, E94.

- [26] N. Kumpan, T. Poonsawat, L. Chaicharoenwimolkul, S. Pornsuwan, E. Somsook, *RSC Advances* **2017**, 7, 5759.
- [27] M. E. Suss, V. Presser, *Joule* **2018**, 2, 10.
- [28] V. D. Neff, *Journal of The Electrochemical Society* **1978**, 125, 886.
- [29] a) K. R. Dunbar, R. A. Heintz, in *Progress in Inorganic Chemistry*, Vol. 45 (Ed: K. D. Karlin), John Wiley and Sons, USA **1996**, p. 283; b) J. F. Keggin, F. D. Miles, *Nature* **1936**, 137, 577; c) D. F. Shriver, in *Structure And Bonding*, Vol. 1, Springer-Verlag Berlin Heidelberg, Germany **1966**, p. 32.
- [30] a) F. Scholz, H. Kahlert, in *Encyclopedia of Electrochemistry*, DOI: 10.1002/9783527610426.bard070023 (Ed: A. J. Bard), Wiley-VCH **2007**, p. 701; b) K. Hurlbutt, S. Wheeler, I. Capone, M. Pasta, *Joule* **2018**, 2, 1950.
- [31] C. D. Wessells, S. V. Peddada, R. A. Huggins, Y. Cui, *Nano Letters* **2011**, 11, 5421.
- [32] a) N. R. de Tacconi, K. Rajeshwar, R. O. Lezna, *Chemistry of Materials* **2003**, 15, 3046; b) M. Pyrasch, A. Toutianoush, W. Jin, J. Schnepf, B. Tieke, *Chemistry of Materials* **2003**, 15, 245; c) K. Itaya, I. Uchida, V. D. Neff, *Accounts of Chemical Research* **1986**, 19, 162.
- [33] R. Y. Wang, C. D. Wessells, R. A. Huggins, Y. Cui, *Nano Letters* **2013**, 13, 5748.
- [34] A. Nilchi, R. Saberi, M. Moradi, H. Azizpour, R. Zarghami, *Chemical Engineering Journal* **2011**, 172, 572.
- [35] A. A. Karyakin, O. V. Gitelmacher, E. E. Karyakina, *Analytical Letters* **1994**, 27, 2861.
- [36] S. Ferlay, T. Mallah, R. Ouahès, P. Veillet, M. Verdaguer, *Nature* **1995**, 378, 701.
- [37] K. Itaya, K. Shibayama, H. Akahoshi, S. Toshima, *Journal of Applied Physics* **1982**, 53, 804.
- [38] a) V. D. Neff, *Journal of The Electrochemical Society* **1985**, 132, 1382; b) C. D. Wessells, R. A. Huggins, Y. Cui, *Nature Communications* **2011**, 2, 550.
- [39] a) N. A. Sitnikova, M. A. Komkova, I. V. Khomyakova, E. E. Karyakina, A. A. Karyakin, *Analytical Chemistry* **2014**, 86, 4131; b) K. Itaya, H. Akahoshi, S. Toshima, *Journal of The Electrochemical Society* **1982**, 129, 1498.
- [40] a) M. A. Lila, R. J. Orth, J. P. H. Sukanto, S. M. Haight, D. T. Schwartz, *Separation and Purification Technology* **1997**, 11, 147; b) W. Chen, X. H. Xia, *Advanced Functional Materials* **2007**, 17, 2943; c) R. Chen, H. Tanaka, T. Kawamoto, M. Asai, C. Fukushima, M. Kurihara, M.

- Ishizaki, M. Watanabe, M. Arisaka, T. Nankawa, *ACS Applied Materials & Interfaces* **2013**, *5*, 12984.
- [41] S. Porada, A. Shrivastava, P. Bukowska, P. M. Biesheuvel, K. C. Smith, *Electrochimica Acta* **2017**, *255*, 369.
- [42] a) O. Lefebvre, R. Moletta, *Water Research* **2006**, *40*, 3671; b) Y. Xiao, D. J. Roberts, *Environmental Technology* **2010**, *31*, 1025.
- [43] a) J. Qiao, Y. Liu, F. Hong, J. Zhang, *Chemical Society Reviews* **2014**, *43*, 631; b) N.-T. Suen, S.-F. Hung, Q. Quan, N. Zhang, Y.-J. Xu, H. M. Chen, *Chemical Society Reviews* **2017**, *46*, 337; c) M. Zeng, Y. Li, *Journal of Materials Chemistry A* **2015**, *3*, 14942.
- [44] X. Mao, F. Simeon, D. S. Achilleos, G. C. Rutledge, T. A. Hatton, *Journal of Materials Chemistry A* **2013**, *1*, 13120.
- [45] T. Kim, M. Rahimi, B. E. Logan, C. A. Gorski, *Environmental Science & Technology* **2016**, *50*, 9791.
- [46] C. D. Wessells, M. T. McDowell, S. V. Peddada, M. Pasta, R. A. Huggins, Y. Cui, *ACS Nano* **2012**, *6*, 1688.
- [47] Y. You, X.-L. Wu, Y.-X. Yin, Y.-G. Guo, *Journal of Materials Chemistry A* **2013**, *1*, 14061.
- [48] S. Ayrault, B. Jimenez, E. Garnier, M. Fedoroff, D. J. Jones, C. Loos-Neskovic, *Journal of Solid State Chemistry* **1998**, *141*, 475.
- [49] S. J. Gerber, E. Erasmus, *Materials Chemistry and Physics* **2018**, *203*, 73.
- [50] a) L. Xia, R. L. McCreery, *Journal of The Electrochemical Society* **1999**, *146*, 3696; b) C. M. Pharr, P. R. Griffiths, *Analytical Chemistry* **1997**, *69*, 4665.
- [51] Y. Maréchal, *The Journal of Chemical Physics* **1991**, *95*, 5565.
- [52] C.-C. Yang, Y.-C. Lin, P.-I. Wang, D.-J. Liaw, S.-W. Kuo, *Polymer* **2014**, *55*, 2044.
- [53] a) L. F. Schneemeyer, S. E. Spengler, D. W. Murphy, *Inorganic Chemistry* **1985**, *24*, 3044; b) J. Joseph, H. Gomathi, G. Prabhakara Rao, *Electrochimica Acta* **1991**, *36*, 1537; c) S. Sinha, B. D. Humphrey, A. B. Bocarsly, *Inorganic Chemistry* **1984**, *23*, 203; d) A. B. Bocarsly, S. Sinha, *Journal of Electroanalytical Chemistry and Interfacial Electrochemistry* **1982**, *140*, 167.
- [54] M. Bárcena Soto, F. Scholz, *Journal of Electroanalytical Chemistry* **2002**, *521*, 183.
- [55] F. Scholz, A. Dostal, *Angewandte Chemie International Edition in English* **1996**, *34*, 2685.

- [56] P. J. Kulesza, M. A. Malik, R. Schmidt, A. Smolinska, K. Miecznikowski, S. Zamponi, A. Czerwinski, M. Berrettoni, R. Marassi, *Journal of Electroanalytical Chemistry* **2000**, 487, 57.
- [57] S. J. Reddy, A. Dostal, F. Scholz, *Journal of Electroanalytical Chemistry* **1996**, 403, 209.
- [58] N. F. Zakharchuk, N. Naumov, R. Stösser, U. Schröder, F. Scholz, H. Mehner, *Journal of Solid State Electrochemistry* **1999**, 3, 264.
- [59] J. F. Bertrán, J. B. Pascual, M. Hernández, R. Rodríguez, *Reactivity of Solids* **1988**, 5, 95.
- [60] M. Pasta, C. D. Wessells, R. A. Huggins, Y. Cui, *Nature Communications* **2012**, 3, 1149.
- [61] N. G. Connolly, W. E. Geiger, *Chemical Reviews* **1996**, 96, 877.
- [62] K. M. Jeerage, D. T. Schwartz, *Separation Science and Technology* **2000**, 35, 2375.
- [63] United States Environmental Protection Agency, in *National Primary Drinking Water Regulations EPA 816-F-09-004*, 2009.
- [64] United States Environmental Protection Agency, in *2018 Edition of the Drinking Water Standards and Health Advisories Tables EPA 822-F-18-001*, 2018.
- [65] a) M. T. Pope, A. Müller, *Angewandte Chemie International Edition in English* **1991**, 30, 34; b) S.-S. Wang, G.-Y. Yang, *Chemical Reviews* **2015**, 115, 4893.
- [66] K. Weissrnel, H. Arpe, in *Industrial Organic Chemistry*, DOI: 10.1002/9783527619191.ch8 (Eds: K. Weissrnel, H. Arpe), Wiley-VCH, Weinheim **2008**, p. 193.
- [67] D. J. Cole-Hamilton, *Science* **2003**, 299, 1702.
- [68] H.-W. Lee, M. Pasta, R. Y. Wang, R. Ruffo, Y. Cui, *Faraday Discussions* **2014**, 176, 69.
- [69] L. Pettersson, I. Andersson, L. O. Oehman, *Inorganic Chemistry* **1986**, 25, 4726.
- [70] E. A. Nagul, I. D. McKelvie, P. Worsfold, S. D. Kolev, *Analytica Chimica Acta* **2015**, 890, 60.
- [71] F. Ju, D. VanderVelde, E. Nikolla, *ACS Catalysis* **2014**, 4, 1358.
- [72] M. T. Pope, in *Polyoxometalate Molecular Science*, DOI: 10.1007/978-94-010-0091-8\_1 (Eds: J. J. Borrás-Almenar, E. Coronado, A. Müller, M. Pope), Springer Netherlands, Dordrecht **2003**, p. 3.
- [73] B. Karwowska, P. J. Kulesza, *Electroanalysis* **1995**, 7, 1005.